RESEARCH ARTICLE

INTERNATIONAL RESEARCH JOURNAL OF MULTIDISCIPLINARY TECHNOVATION

Asian Research Association

DOI: 10.54392/irjmt2639

Design and Analysis of a Compact Multi Input Multi Output Truncated Circular Planar Antenna using Defected Ground Structure for Millimeter Applications

M. Jyothirmai [a, b, *], T. Tirupal [c]

[a] Jawaharlal Nehru Technological University, Anantapur, Ananthapuramu, Andhra Pradesh, India
[b] Ravindra College of Engineering for Women, Kurnool, Andhra Pradesh, India.
[c] G. Pullaiah college of Engineering and Technology, Kurnool, Andhra Pradesh, India
* Corresponding Author Email: mamanijyothirmai23@gmail.com

DOI: https://doi.org/10.54392/irjmt2639
Received: 26-12-2025; Revised: 23-04-2026; Accepted: 30-04-2026; Published: 08-05-2026

Abstract: A novel planar multi-input multi output (MIMO) antenna operating at 28 GHz is proposed, featuring a four-elements with rotationally symmetric circular resonators with defected ground plane (DGP) to enhance performance of gain and isolation. The single element circular patch antenna design is extended into a MIMO configuration to improve gain and directivity, making it suitable for 5G. The proposed antenna is analyzed through simulated S-parameters, including S_{11} (like the single-element antenna) and S_{21}, S_{31} for the MIMO configuration for evaluate impedance matching and coupling effects using the commercially available CST microwave studio suite software. A very fine mesh size used in the simulation for better accuracy for getting the good simulation results. The radiation characteristics at the resonant frequency are examined using both polar and 3D radiation patterns, demonstrating the antenna directional behavior and effective radiation performance. The antenna structure overall size is 45 x 45 x 0.254 mm3. The Rogers 5880 with 2.2 dielectric constant is used as the substrate for the material. The defected ground plane (DGP) is used to improve the isolation between the ports in the MIMO structure. The proposed work examined in terms of the parameters like S11, S21, ECC (Envelope correlation coefficient), DG (Diversity Gain), CCL (Channel capacity Loss), TARC (Total Active Reflection Coefficient) and the radiation pattern. The mutual coupling/isolation is >25 dB and the MIMO parameters i.e., ECC <0.00033 with a DG >9.9 dB is achieved. The antenna is fabricated using photolithography techniques and validated using the vector network analyzer (VNA). Both the simulation and measured results are in good agreement in terms of S-parameters as well as radiation characteristics.

Keywords: MIMO, DGP, BW, DG and ECC.

1. Introduction

In the modern era, rapid proliferation of wireless devices, limited bandwidth and constrained channel capacity have significantly driven the development of advanced communication network standards. This evolution has led to the emergence of next-generation communication systems like 5G as well as 6G, which offer substantially higher data rates and enhanced channel capacity [1-2]. 5G technology aims to deliver improved reliability, high-speed connectivity, and low power consumption to accommodate the exponential growth of connected devices. Moreover, it promises to support emerging technologies such as smart cities and the Internet of Things (IoT) [3-4]. Despite these advantages, mm-wave communications face inherent challenges including signal fading, atmospheric absorption, and high path loss issues that are especially pronounced in single antenna systems [5-6]. To address these limitations multiple-input multiple-output (MIMO) antenna systems have emerged as a key enabler for current and future wireless networks. MIMO technology leverages multiple antennas to enhance channel capacity and enable high data throughput in the gigabits per second (Gbps) [7]. However, 5G MIMO antennas require wide bandwidths, high gain to mitigate atmospheric losses, and compact designs suitable for integration into various devices. The MIMO antenna design challenges such as minimizing mutual coupling and achieving high isolation between closely spaced antenna elements critical factors that impact overall performance.

A wide array of antenna solutions operating at mm-wave frequencies for 5G applications has recently been reported [12]. Some of these designs demonstrate

limited gain [8-9], making them inadequate to overcome the high attenuation experienced at mm-wave frequencies. To combat such propagation losses, several high gain and beam steering antenna arrays have been proposed with strong signal coverage and broad spatial range [10-12]. However, many multi-element antenna arrays are limited by single-port feeding, resulting in performance comparable to single antennas, but the MIMO systems provide advantages such as multipath propagation, increased link reliability, higher capacity, and improved data rates are the core attributes of 5G systems. Different MIMO antenna designs tailored for mm-wave 5G communication have recently been introduced [13-25]. For instance, a planar inverted-F antenna (PIFA) MIMO configuration offering 1 GHz bandwidth and a simulated peak gain of 12 dBi is presented in [12]. A MIMO antenna with an electromagnetic bandgap (EBG) structure, achieving a bandwidth of 0.8 GHz is implemented in [13]. The patch antenna was selected due to low-profile and planar structure, suitable for compact integration, ease of fabrication at mm-wave frequencies as well as compatibility with MIMO configurations and array structures and better integration capability compared to PIFA and DRA involves more complex geometries. In [14], a multi-element antenna capable of directional radiation suitable for 5G applications is proposed, achieving 1.5 GHz bandwidth (27.2–28.7 GHz) and a peak gain of 7.41 dBi at 28 GHz.

Dielectric resonator antennas (DRAs) for 5G applications are explored in [15,16], with bandwidths near 1 GHz. Reference [15] employs a substrate-integrated waveguide (SIW) feed with a peak gain of 7.37 dBi, while [16] evaluates envelope correlation coefficient (ECC) to assess MIMO performance. Similarly, [17] presents a slotted SIW-fed MIMO antenna array covering 24.25–27.5 GHz and 27.5–28.35 GHz, with gains ranging from 8.2 to 9.6 dBi. In [18], a compact T-shaped four-element MIMO antenna (dimensions: 12×50.8×0.8 mm³) offers wide bandwidth (25.1–37.5 GHz) and a peak gain of 10.6 dBi, although only ECC is analyzed. An 8×8 MIMO array with a 31.2×31.2×1.57 mm³ substrate is presented in [19], resonating at 25.2 GHz with a 5.68 GHz bandwidth and a peak gain of 8.732 dBi. ECC, mean effective gain (MEG), and diversity gain (DG) are evaluated. In [20] introduces a two-port MIMO array (31.7×53×0.2 mm³) with microstrip feedlines and EBG reflectors, achieving wide bandwidth and peak gain up to 11.5 dBi. MIMO performance is evaluated through ECC and DG. A MIMO antenna with integrated metamaterial arrays is demonstrated in [22], with a 30×30.5×0.508 mm³ substrate and a peak gain of 7.4 dBi at 26 GHz.

Table 1 summarizes the antenna structures along with their advantages and limitations in the literature. It is observed that while various techniques such as metamaterials, DGS and array configurations improve gain, bandwidth and isolation but they often introduce increased design complexity, fabrication challenges and size constraints. Therefore, achieving a compact, wideband, and high-isolation antenna suitable for 5G applications remains a significant research challenge.

In this paper, we propose the design of a four-element circular patch array with MIMO capabilities for mm-wave 5G frequency bands. The proposed antenna features high gain and well-suited for next-generation devices such as smartwatches and mobile systems. With its compact and straightforward geometry, the antenna design supports seamless integration into 5G-enabled smart devices. Its excellent MIMO performance affirms its suitability for future 5G wireless communication applications.

Table 1. Summary of the Literature

Ref No	Antenna structure	Advantage	Disadvantage
[5]	mmWave antenna arrays	High gain, beam steering capability	Complex feeding network, high cost
[8]	Switched beam antenna (PIN diodes)	Bean steering and adaptive radiation	Biasing complexity and losses.
[12]	PIFA MIMO	Compact and suitable for mobile devices	Limited Bandwidth
[13]	EBG-backed MIMO antenna	Reduced mutual coupling, improved isolation	Increased thickness and fabrication complexity
[15]	Substrate integrated dual frequency antenna	Compact, dual band operation	Limited bandwidth
[16]	Dielectric resonator MIMO	High efficiency and low loss	Complex fabrication and integration issues
[18]	T-shaped DGS MIMO antenna	Improved isolation and compact	Design sensitivity to parameters
[19]	MIMO antennas for 5G devices	Enhanced capacity, diversity gain	Mutual coupling challenges
[25]	4-port DGS MIMO antenna	Good isolation, compact design	Increased design complexity

2. Antenna Design

The antenna was designed using the low loss laminate i.e. Rogers 5880 with εr = 2.2 and a thickness/height of 0.254 mm. The rogers 5880 have used in high-frequency applications, minimum dielectric losses and is commercially available. The overall size of the proposed circular patch MIMO antenna is 45 mm × 45 mm × 0.254 mm. The design consists of four circular patch radiating elements. The microstrip line is used as feed for excite the MIMO antennas. The quarter wave transformer is used for impedance matching between the circular patch and microstrip feed line. The distance between the two circular patch elements in the MIMO antenna configuration is 20 mm and the circular patch diameter is 7.4 mm. All the dimensions of the proposed antenna are represented in table 2. The proposed truncated circular patch antenna is design procedure is represented in figure 1. The figure 1 (a) is represented basic circular patch with microstrip line feed technique. For better impedance matching of the antenna impedance transformer technique is implemented and is represented in figure 1(b). The proposed truncated circular patch antenna is represented in the figure 1(c). The DGP is used to enhance the isolation and performance of the proposed MIMO antenna. The circular patch used in the proposed design the radius of the patch (a) is calculated using the following expression.

$$a = \frac{F}{\left\{1+\frac{2h}{\pi\varepsilon_r}\left[\ln\left(\frac{\pi F}{2h}\right)+1.7726\right]\right\}^{1/2}} \quad (1)$$

Where, $F = \frac{8.791\times10^9}{f_r\sqrt{\varepsilon_r}}$, f_r is the resonant frequency of the application, h is the substrate height, ε_r is the dielectric permittivity/constant of the substrate. The effective radius (a_{eff}) due to fringing fields is

$$\alpha_{eff} = \alpha\sqrt{1+\frac{2h}{\pi\varepsilon_r}\left[\ln\left(\frac{\pi\alpha}{2h}\right)+1.7726\right]} \quad (2)$$

The input impedance at the edge of the feed line is

$$R_{in} = \frac{1}{2Gl} \quad (3)$$

Where $Gl = \frac{1}{120\pi^2\int_0^{\pi}\left[\frac{\sin(k_0 a\cos\theta)}{\cos\theta}\right]^2}$

By incorporating slots in the circular patch, the effective radius is

$$a'_{eff} = a_{eff} - \Delta a \quad (4)$$

Where Δa is the reduction of area due to slots, then the resonant frequency shift $f'_r = \frac{X_{mn}C}{2\pi a'_{eff}\sqrt{\varepsilon_r}}$ where X_{mn} is the mode constant.The equivalent LC model for the proposed structure is

$$f_r = \frac{1}{2\pi\sqrt{L_{eq}C_{eq}}} \quad (5)$$

Where Leq and Ceq are the equivalent inductance and capacitance of the structure. The introduction of slots in the radiating structure can be represented by an equivalent LC circuit, where the inductance increases due to the change of the surface current path, and the capacitance increases due to the slot gaps. This combined effect reduces the resonant frequency and enables antenna miniaturization.

The design and optimization procedure of the proposed antenna is represented in figure 2. The Figure 3 is the proposed compact 2x2 circular patch MIMO antenna, each element is fed in different orientations to achieve polarization diversity and improves channel capacity.

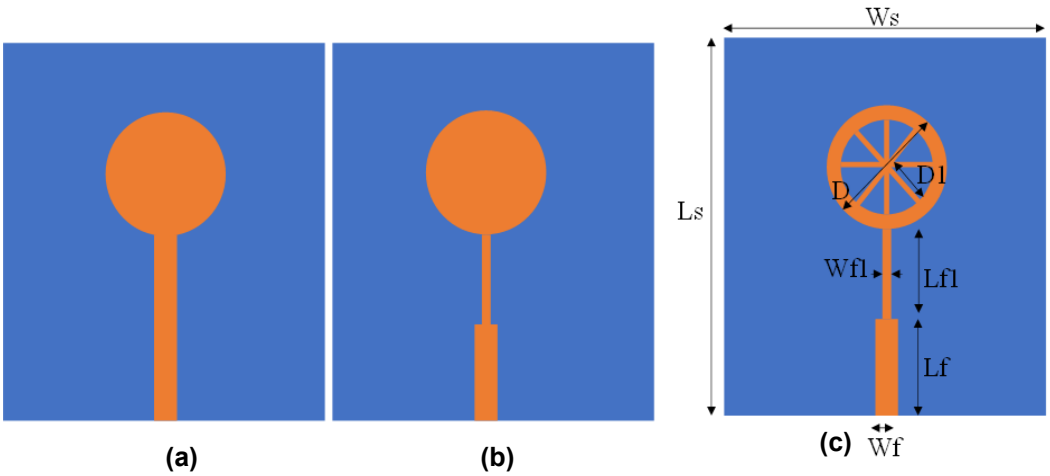

Figure 1. Single element antenna design procedure **(a)** antenna 1 (circular patch with microstrip line) **(b)** antenna 2 (circular patch with impedance transformer) and **(c)** Truncated circular patch antenna.

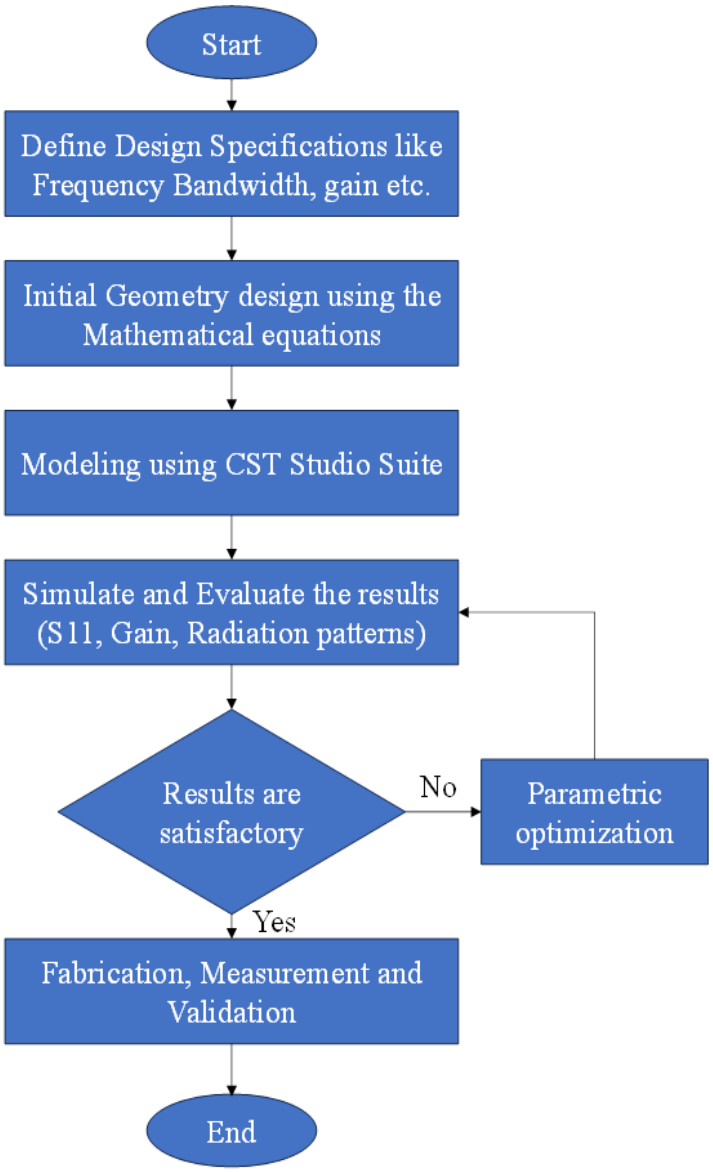

Figure 2. Design and Optimization Block diagram of the proposed antenna

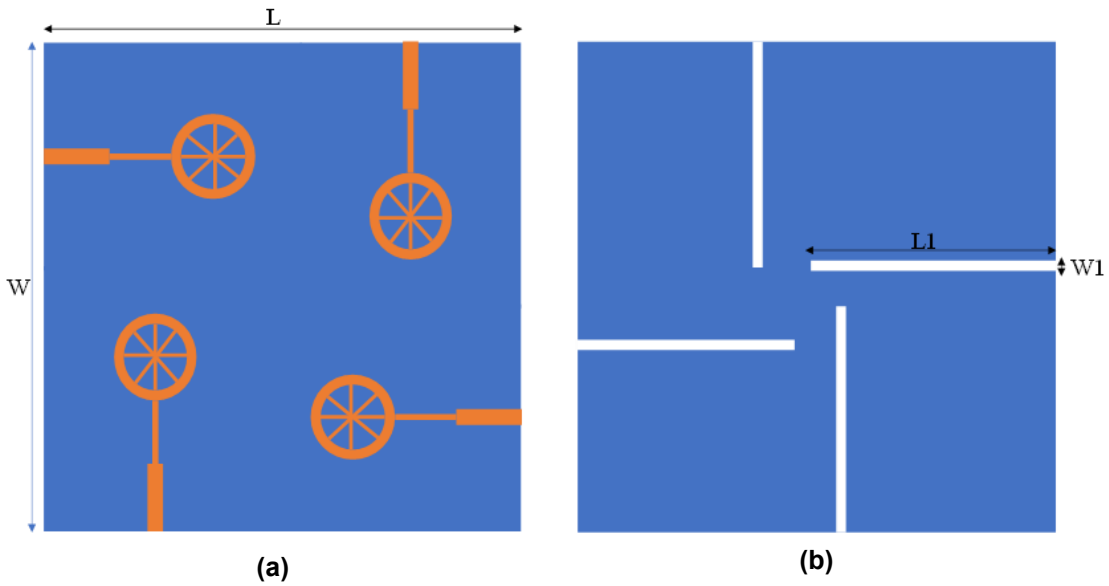

Figure 3. Proposed 2X2 MIMO antenna with DGP **(a)** Front view **(b)** Back view

Table 2. Antenna design parameters

S. No	Parameter	Value (mm)	S. No	Parameter	Value (mm)
1	Ls	25	7	D	7.4
2	Ws	20	8	D1	7.1
3	Lf	6	9	L	45
4	Wf	0.75	10	W	45
5	Lf1	5	11	L1	20
6	Wf1	0.1	12	W1	1

The antenna is designed to operate in the frequency range of 28 GHz which comes under 5G millimeter applications. The design and analysis of the proposed 2x2 circular patch MIMO antenna was carried out using commercially available antenna design software i.e. CST (computer simulation technology) studio suite.

3. Simulation Results

The return loss (S11) of the antenna 1, antenna 2 and truncated circular patch antenna is represented in figure 4. The proposed single element has a bandwidth of >270 MHz with impedance of 50 ohms. The 2x2 MIMO antenna simulation results of S1, S22, S33, S44 and isolation (S21, S31, S41), VSWR and radiation pattern of the proposed MIMO antenna was analyzed using a CST studio suite. The simulation result of S11 and VSWR are represented in the Figure 4 and 5 respectively. The $|S_{11}|$ result represents that antenna is resonating at 28 GHz frequency with a bandwidth of 0.278 GHz. The proposed single element simulated $|S_{11}|$ remained below –10 dB across the required operating frequency range and the minimum value observed from figure 3 is ~17 dB at 28 GHz.

The figure 5 represents the simulation results of the proposed 2x2 MIMO antenna with truncated circular patch with DGP. The simulated S-parameter results of the proposed 2x2 MIMO dual-polarized mm Wave antenna array, operating in the 26–30 GHz band, are shown in Figure 5. The return loss parameters (S_{11}, S_{22}, S_{33}, S_{44}) exhibit a sharp resonance around 28 GHz, with values below –10 dB which indicating good impedance matching across all ports. The mutual coupling parameters (S_{21}, S_{31}, S_{41}, S_{32}) demonstrate excellent isolation performance, with S_{31} achieving levels better than –50 dB over most of the frequency range, and the remaining coupling terms consistently below –25 dB. This high isolation is attributed to the orthogonal feed arrangement and the incorporation of the DGP, which effectively suppresses surface wave coupling. The array achieves symmetrical performance across all ports, confirming the balanced design and suitability for dual-polarized 2x2 MIMO operation in the 28 GHz 5G mm Wave band.

Figure 6 represents the simulated radiation characteristics of the proposed 2x2 MIMO antenna at 28 GHz frequency with each port excited individually while the remaining ports are terminated with matched loads. The figure 6(a)-(d) represents H-plane phi = 0 degree and these plots contains a beamwidth of 39.1 degrees. The figure 6(e)-(h) represents E-plane phi = 90 degree and these plots contains a beamwidth of 37.3 degrees with a SLL<-15 dB. The 3D radiation patterns exhibit broad and stable radiation coverage with distinct main lobes, where red regions represent maximum gain and green/blue indicate lower intensity in the figure 6(i) –(l). The quasi-omnidirectional nature of the lobes, combined with symmetrical distribution across ports, ensures wide angular coverage and effective polarization diversity. These characteristics, along with minimal pattern distortion, confirm the suitability of the array for 28 GHz MIMO applications. The gain achieved in the simulation is >9.3 dB across all the 4 ports of the proposed antenna. The gain versus frequency of the proposed antenna is represented in figure 7.

The truncated circular patch is shown to improve impedance matching and bandwidth enhancement. The DGP is demonstrated to enhance port isolation by suppressing surface current coupling. A comparative discussion with existing MIMO antenna designs has been added to emphasize the performance improvements achieved.

The surface current distribution for the proposed antenna in the figure 8 clearly demonstrates the role of the DGP in enhancing antenna performance. With the introduction of DGP, the current distribution becomes more concentrated and spreads along the wheel structure region, resulting in extended current paths. This increase in effective current path length enhances the equivalent inductance, while the slot gaps introduce additional capacitance.

Furthermore, the DGP suppresses surface wave propagation, thereby reducing mutual coupling and improving isolation characteristics.

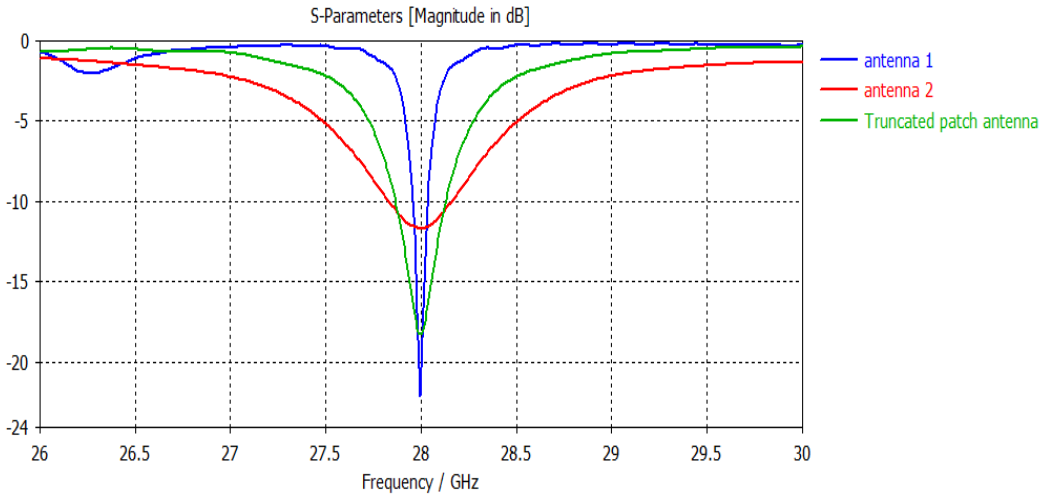

Figure 4. Return loss (S11) of the single element antenna

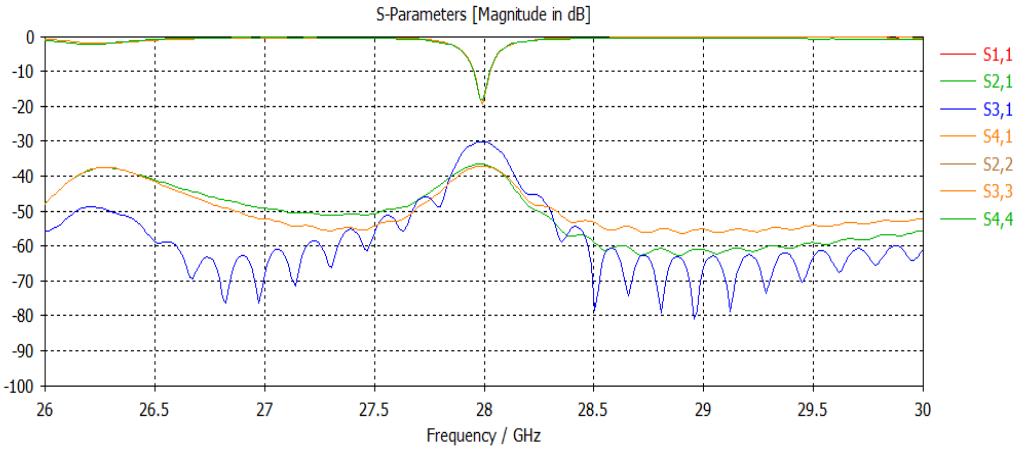

Figure 5. S-parameter characteristics of the proposed 2X2 MIMO antenna

These effects collectively validate the effectiveness of the proposed DGP in improving the overall antenna performance.

The comparison parameters of the proposed 2x2 MIMO antenna with the corresponding 2x2 MIMO antenna with basic circular patch, wheel type structure and the proposed antenna in terms of bandwidth, gain and port to port isolation is represented in table 3.

4. Measured Results

The figure 9 represents the fabricated prototype of the proposed 2x2 MIMO antenna. The structure consists of four truncated circular patch antenna with wheel-shaped slots, arranged in the 2×2 configuration. The feed lines are oriented orthogonally; two elements are fed horizontally and two fed vertically to meet the polarization diversity. This configuration helps improve polarization diversity and reduce mutual coupling between. The fabricated layout and feed arrangement are optimized for operation around 28 GHz for MIMO applications. The MIMO antenna is fabricated using the photolithographic techniques and commercially available fabrication process. The fabricated prototype is tested using the Agilent Keysight VNA (N5230A) using the suitable calibration kit. The 0.25 mm SMA connectors are used for the fabrication and very fine solder used for soldering the microstrip line and the thick lead was used for the ground to properly grounded as well as return path for the signal. While measuring the port 1 and port 2 return loss and isolation, the other two ports are terminated using the 50-ohm terminations.

The measure s-parameters like return loss (S11, S22, S33, S44) and isolation parameter (S21, S31 and S41) of the fabricated model is represented in figure 9. The simulated and measured s-parameters are in good agreement. From the figure 9, it is observed that MIMO antenna covers 27.8-28.2 GHz with return loss is <-10 dB across all the four ports. The minimum isolation is observed in the measured results are <-25 dB. For simulation and measured s-parameters compared and represented in the figure 11.

The measured E-field (phi=90 degrees) and H-field (phi= 0 degrees) radiation pattern at 28 GHz is represented in figure 12. The radiation pattern is measured using the anechoic chamber.

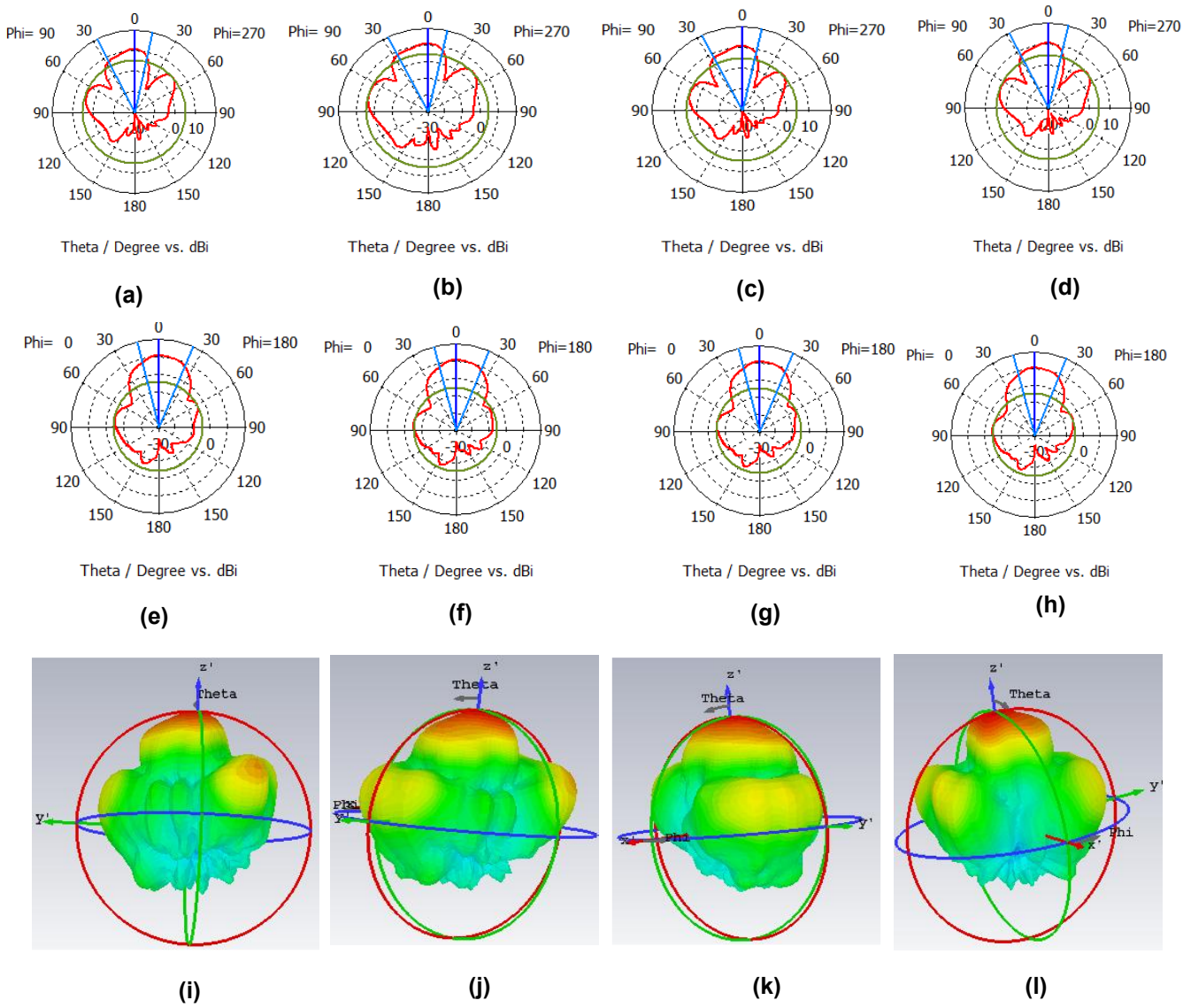

Figure 6. Simulated Radiation characteristics of the proposed 2 by 2 MIMO antenna across all the 4 ports. The (a-d) represents H-plane, (e-h) represents E-plane and (j-l) represents 3D radiation pattern across all 4 ports excitation

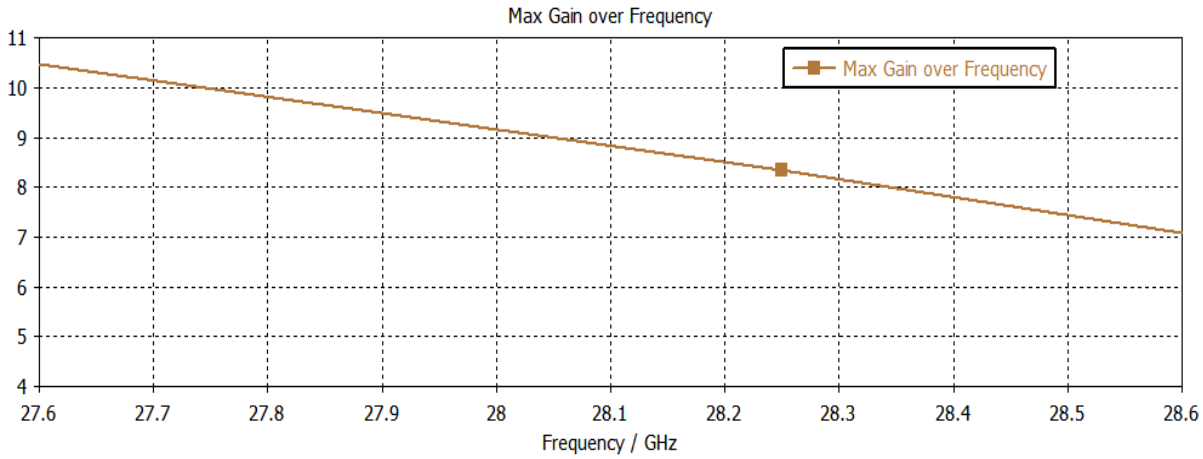

Figure 7. Gain versus Frequency plot for the proposed 2x2 MIMO antenna

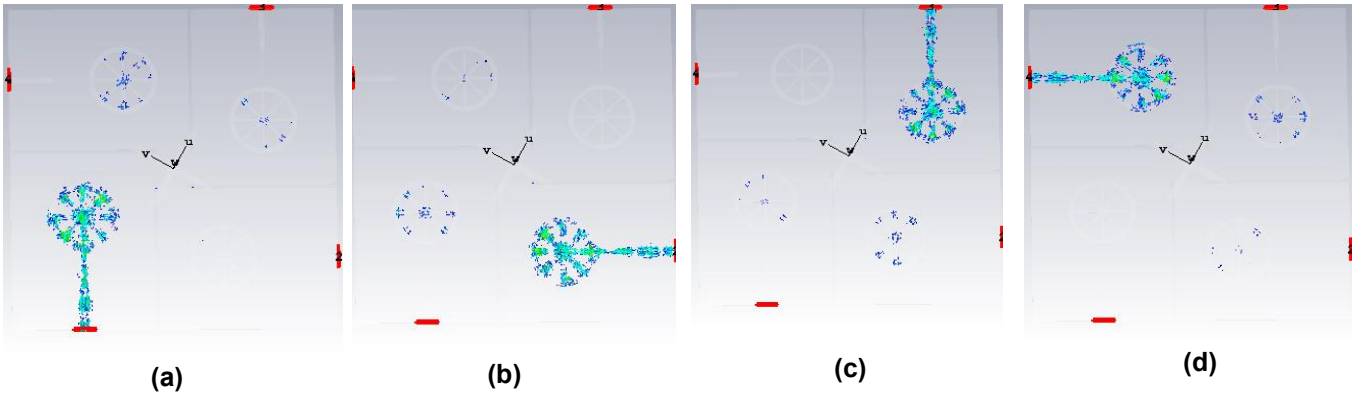

Figure 8. Surface current distributions of the 2 by 2 MIMO antenna **(a)** port 1 **(b)** port 2 **(c)** port 3 and **(d)** port 4.

Table 3. Comparison results of the proposed 2x2 MIMO antenna with intermediate stage of antennas

Antenna	Bandwidth (GHz)	Gain	Port to port isolation (dB)
MIMO basic antenna	0.2	7	15
Wheel type MIMO antenna	0.27	9	22
Proposed Wheel type MIMO antenna with DGP	0.278	9.3	30

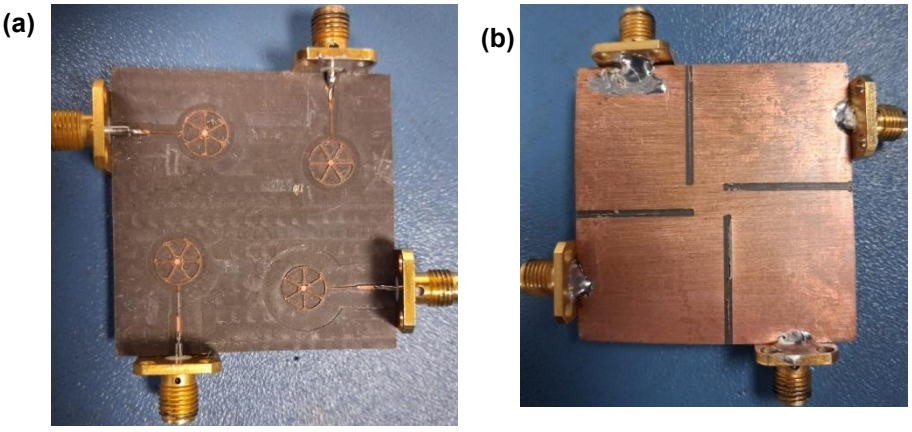

Figure 9. Fabricated prototypes of the proposed antenna 2x2 MIMO antenna **(a)** top view of radiating element and **(b)** Back view of the DGP.

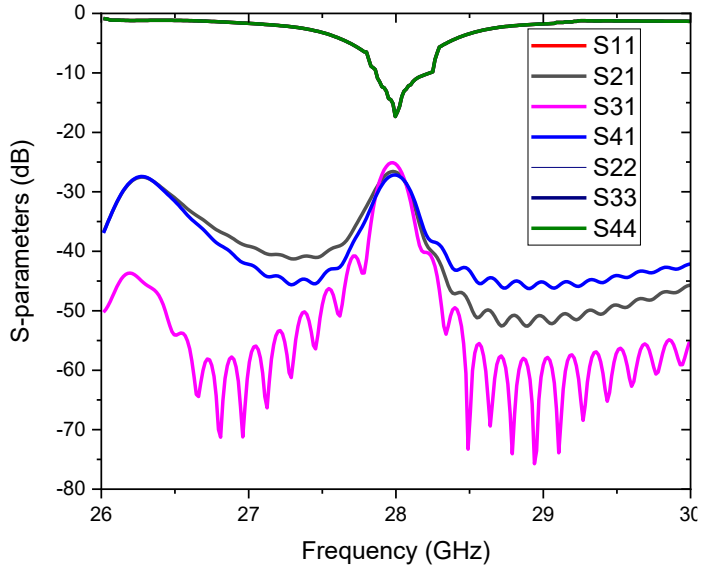

Figure10. Measured S-parameter characteristics of the proposed 2X2 MIMO antenna

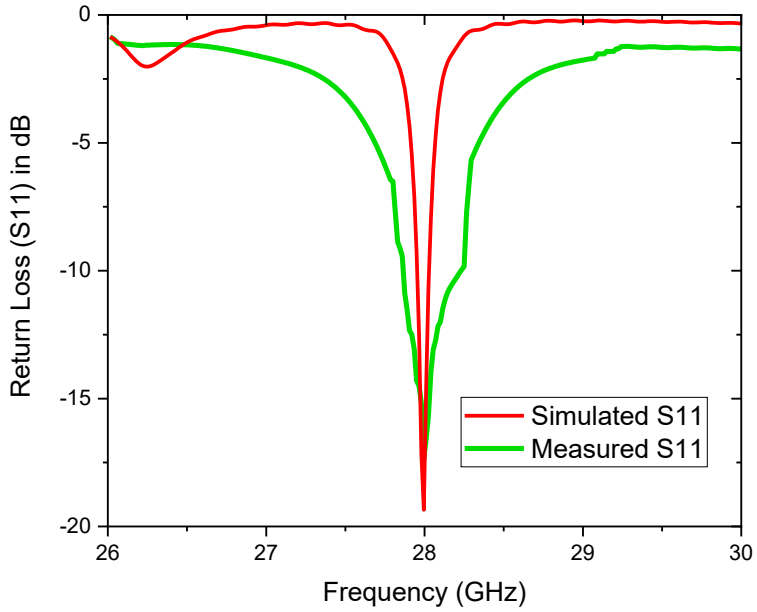

Figure 11. The simulated versus measured Return Loss parameter of the proposed 2x2 MIMO antenna.

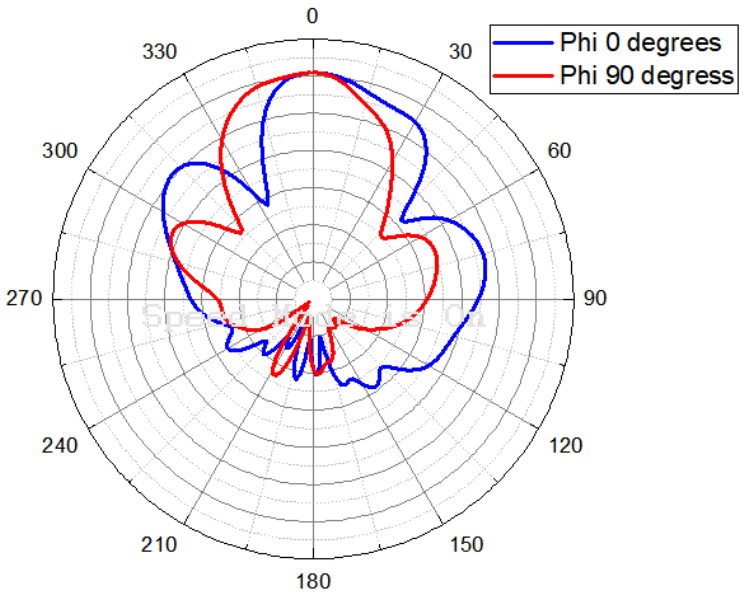

Figure 12. Measured Radiation pattern at 28 GHz

5. MIMO Parameters

To ensure the performance of the MIMO antenna, it is essential to consider not only the S-parameters and radiation characteristics but also specific diversity parameters. These parameters must meet certain predefined thresholds to ensure the antenna's suitability for practical MIMO applications. This section discusses the key diversity metrics relevant to MIMO antenna evaluation i.e. ECC and DG.

The ECC is quantifies the correlation between signals received at different ports of a MIMO antenna. It is a key metric for assessing channel diversity and quality. A high ECC indicates strong correlation and low isolation between antenna elements, which can significantly degrade overall system performance. ECC reflects the mutual influence of the S-parameters and provides insight into the spatial diversity performance of the antenna. It can be calculated by use of received signal envelopes, S-parameters, or far-field radiation patterns to estimate complex cross-correlation. In this study, ECC is evaluated using the S-parameter-based approach [23] is shown in the equation (6). The ECC is calculated using S-parameter method is used for practical measurement purposes to simplify the process.

$$ECC = \frac{|s_{ii^*} s_{ij} + s_{ji^*} s_{jj}|^2}{\left(1-|s_{ii}|^2-|s_{ij}|^2\right)\left(1-|s_{jj}|^2-|s_{jj}|^2\right)} \quad (6)$$

Figure 13 illustrates the simulated ECC of the proposed 2x2 MIMO antenna array over the 26–30 GHz band. The ECC values for all port combinations remain extremely low, well below the critical threshold of 0.5, and in most cases under 0.005, confirming excellent isolation and minimal correlation between antenna elements. Such low ECC ensures that the antenna ports operate independently, enabling effective spatial and polarization diversity, which is essential for enhancing MIMO channel capacity and overall link reliability.

The ECC limit for the practical antennas are <0.5 is used for uncorrelated MIMO antennas in [24]. The DG is the another crucial parameter of the MIMO antenna, as it use for reliability and effectiveness of the received signal in multipath environments. The high DG values indicates the better isolation between radiation elements. The DG is enhancing the communication robustness and the isolation between the radiating elements are higher for higher DG antenna systems [25]. The DG of the MIMO antenna is calculated using equation 7 represents below.

$$DG = 10\sqrt{1-(ECC)^2} \tag{7}$$

The figure 14 shows the DG performance of the proposed 2x2 MIMO antenna across the frequency range of 26-30 GHz. The DG values remain consistently close to the ideal 10 dB throughout the band, demonstrating the array's high diversity efficiency. Only minor variations are observed below 27 GHz, which are negligible and have no significant impact on system performance. The combination of near-ideal DG and very low ECC confirms the suitability of the proposed MIMO antenna has high-capacity and reliable 28 GHz MIMO communications.

The Channel Capacity Loss (CCL) and Total Active Reflection Coefficient (TARC) are evaluated the MIMO performance of the proposed antenna. The CCL is computed from the S-parameter-based correlation matrix, and the value is below 0.4 bits/s/Hz, which indicates minimal capacity degradation. The TARC is calculated by considering simultaneous excitation of all ports with varying phase differences, providing a realistic measure of reflection characteristics. The CCL is calculated using the below equation,

$$CCL = -\log_2 det(\varphi^R) \tag{8}$$

Where, $\varphi^R = \begin{bmatrix} \varphi_{ii} & \varphi_{ij} \\ \varphi_{ji} & \varphi_{jj} \end{bmatrix}$ $\varphi_{ii} = 1-(|S_{ii}|^2+|S_{ij}|^2$, $\varphi_{ij} = -(S_{ii}*S_{ij}+S_{ji}*S_{jj})$,

$\varphi_{ji} = -(S_{ii}*S_{ij}+S_{ji}*S_{jj})$, and $\varphi_{jj} = 1-(|S_{jj}|^2+|S_{ji}|^2$. Here the ψ^R is correlation matrix of the receiving antenna.

The TARC is calculated using the below formula

$$\text{TARC} = \frac{\sqrt{(|S_{ii}+S_{ji}\,e^{j\theta}|^2+(|S_{ji}+S_{jj}\,e^{j\theta}|^2)^2}}{\sqrt{2}} \tag{9}$$

The CCL and TARC value are calculated as 0.23 and -16.3 respectively. The obtained results confirm good isolation, low correlation, and efficient multi-port operation of the proposed design.

A comparison of related works represented in the literature are tabulated in table 4. The comparative parameters like operating frequency, size of the antenna, number of ports, Gain, ECC and DG are compared with the proposed MIMO antenna. The MIMO performance of the proposed work exhibits the better performance compared with the reported works in the below table.

The Simulated ECC and DG figures are simulated and are represented in figure 12 and figure 13 respectively.

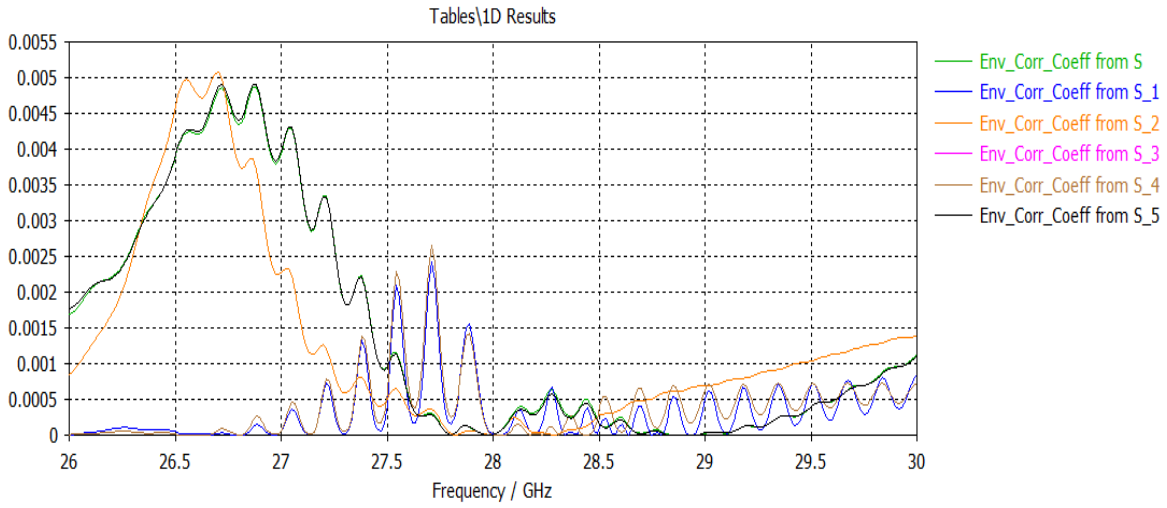

Figure 13. Simulated ECC of the proposed 2x2 MIMO antenna across all the ports.

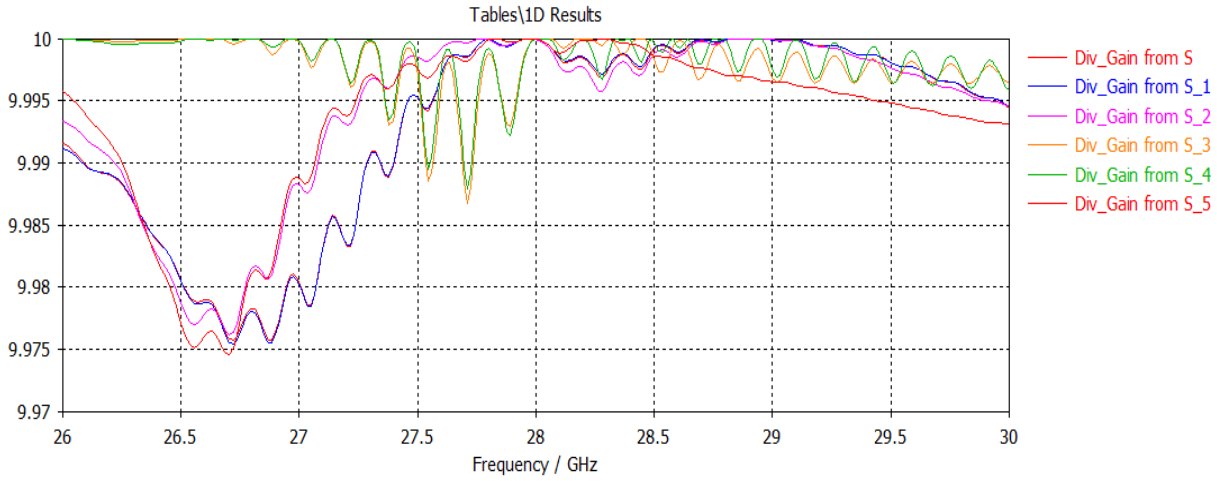

Figure14. Simulated DG of the proposed 2x2 MIMO antenna across all the ports

Table 4. Performance comparison of the proposed antenna with literature

Ref.	Frequency (GHz)	Size of the Antenna (mm^3)	Number of MIMO Ports	Gain (dBi)	ECC, DG (dB)
[8]	3.6	150 × 75 × 1.6	8	2.5	<0.01
[11]	28	41.3 × 46 × 0.508	4	13.1	Not provided
[13]	24	15 × 19 × 0.254	2	7.41	0.24, 9.7
[15]	5.2 & 24	40 × 25 × 0.254	2	5 & 7.37	Not provided
[16]	30	48 × 21 × 0.13	2	>7	<0.4, Not provided
[21]	28	20 × 20 × 0.254	2	8	0.13, 9.9
[25]	28	30 × 35 × 0.76	4	8.3	<0.01, >9.96
This work	28	45 × 45 × 0.254	4	9.7	<0.00033, >9.9

The ECC value and DG values from the simulation are 0.00033 and >9.9, the CCL and TARC value are calculated as 0.23 and -16.3 respectively which represents the proposed antenna is best suitable for the MIMO applications.

6. Conclusion

In this work, a novel planar 2x2 MIMO antenna operating at 28 GHz for 5G and millimeter-wave applications has been designed, optimized and experimentally validated. The proposed design incorporates a four-element patch array integrated with rotationally symmetric truncated circular resonators, which significantly enhance the effective current distribution and contribute to bandwidth improvement and stable radiation characteristics. A DGP is incorporated to suppress surface waves and reduce mutual coupling between closely spaced elements, thereby improving isolation and overall antenna efficiency. The compact antenna occupies a size of 45 45 0.254 mm3 making it suitable for integration into space constrained wireless devices. A peak gain of 9.7 dBi is achieved at the target frequency of 28 GHz, demonstrating strong directional performance. The antenna demonstrates excellent impedance matching, low mutual coupling (>25 dB), and superior MIMO characteristics like ECC <0.00033 and a DG>9.9 dB. Simulated results using CST Microwave Studio has been supported by fine mesh accuracy and closely align with measured data obtained through VNA measurements. Both the simulation and measured results are good agreement and meets the isolation >25 dB in all the ports. The compact structure, high gain, and low correlation make the proposed antenna a strong candidate for integration into future 5G-enabled devices and high-performance mm-wave communication systems.

References

[1] J.G. Andrews, S. Buzzi, W. Choi, S.V. Hanly, A. Lozano, A.C. Soong, J.C. Zhang, What will 5G be?. IEEE Journal on selected areas in communications, 32(6), (2014) 1065-1082. https://doi.org/10.1109/JSAC.2014.2328098

[2] Global Mobile Suppliers Association. (2015). The road to 5G: Drivers, applications, requirements and technical development. A GSA Executive Report from Ericsson, Huawei and Qualcomm.

[3] Z. Pi, F. Khan, An introduction to millimeter-wave mobile broadband systems. IEEE communications magazine, 49(6), (2011) 101-107. https://doi.org/10.1109/MCOM.2011.5783993

[4] T.S. Rappaport, S. Sun, R. Mayzus, H. Zhao, Y. Azar, K. Wang, G.N. Wong, J.K. Schulz, M. Samimi, F. Gutierrez, Millimeter wave mobile communications for 5G cellular: It will work!. IEEE access, 1, (2013) 335-349. https://doi.org/10.1109/ACCESS.2013.2260813

[5] J. Zhang, X. Ge, Q. Li, M. Guizani, Y. Zhang, 5G millimeter-wave antenna array: Design and challenges. IEEE Wireless communications, 24(2), (2016) 106-112. https://doi.org/10.1109/MWC.2016.1400374RP

[6] I. Shayea, T. A. Rahman, M.H. Azmi, M.R. Islam, Real measurement study for rain rate and rain attenuation conducted over 26 GHz microwave 5G link system in Malaysia. IEEE access, 6, (2018) 19044-19064. https://doi.org/10.1109/ACCESS.2018.2810855

[7] N. Ojaroudi Parchin, H. Jahanbakhsh Basherlou, M. Alibakhshikenari, Y. Ojaroudi Parchin, Y.I. Al-Yasir, R.A. Abd-Alhameed, E. Limiti, Mobile-phone antenna array with diamond-ring slot elements for 5G massive MIMO systems. Electronics, 8(5), (2019) 521. https://doi.org/10.3390/electronics8050521

[8] Y. Yashchyshyn, K. Derzakowski, G. Bogdan, K. Godziszewski, D. Nyzovets, C.H. Kim, B. Park, 28 GHz switched-beam antenna based on S-PIN diodes for 5G mobile communications. IEEE Antennas and Wireless Propagation Letters, 17(2), (2017) 225-228. https://doi.org/10.1109/LAWP.2017.2781262

[9] M. Tang, T. Shi, R. W. Ziolkowski, A study of 28 GHz planar multilayered electrically small broadside radiating Huygens source antennas. IEEE Transactions on Antennas and Propagation, 65(12), (2017) 6345–6354. https://doi.org/10.1109/TAP.2017.2700888

[10] N. Yoon, C. Seo, A 28-GHz wideband 2× 2 U-slot patch array antenna. Journal of electromagnetic engineering and science, 17(3), (2017) 133-137. https://doi.org/10.5515/JKIEES.2017.17.3.133

[11] S.X. Ta, H. Choo, I. Park, Broadband printed-dipole antenna and its arrays for 5G applications. IEEE Antennas and Wireless Propagation Letters, 16, (2017) 2183-2186. https://doi.org/10.1109/LAWP.2017.2703850

[12] M. Ikram, Y. Wang, M.S. Sharawi, A. Abbosh, (2018) A novel connected PIFA array with MIMO configuration for 5G mobile applications. In 2018 Australian Microwave Symposium (AMS), IEEE, Australia. https://doi.org/10.1109/AUSMS.2018.8346961

[13] A. Iqbal, A. Basir, A. Smida, N.K. Mallat, I. Elfergani, J. Rodriguez, S. Kim, Electromagnetic bandgap backed millimeter-wave MIMO antenna for wearable applications. IEEE Access, 7, (2019) 111135-111144. https://doi.org/10.1109/ACCESS.2019.2933913

[14] J.S. Park, J.B. Ko, H.K. Kwon, B.S. Kang, B. Park, D. Kim, A tilted combined beam antenna for 5G communications using a 28-GHz band. IEEE Antennas and Wireless Propagation Letters, 15, (2016) 1685-1688. https://doi.org/10.1109/LAWP.2016.2523514

[15] Y. Sun, K.W. Leung, Substrate-integrated two-port dual-frequency antenna. IEEE Transactions on Antennas and Propagation, 64(8), (2026) 3692–3697. https://doi.org/10.1109/TAP.2016.2565740

[16] M.S. Sharawi, S.K. Podilchak, M.T. Hussain, Y.M. Antar, Dielectric resonator based MIMO antenna system enabling millimetre-wave mobile devices. IET Microwaves, Antennas & Propagation, 11(2), (2017) 287-293. https://doi.org/10.1049/iet-map.2016.0457

[17] B. Yang, Z. Yu, Y. Dong, J. Zhou, W. Hong, Compact tapered slot antenna array for 5G millimeter-wave massive MIMO systems. IEEE Transactions on Antennas and Propagation, 65(12), (2017) 6721-6727. https://doi.org/10.1109/TAP.2017.2700891

[18] S.F. Jilani, A. Alomainy, Millimetre-wave T-shaped MIMO antenna with defected ground structures for 5G cellular networks. IET Microwaves, Antennas and Propagation, 12(5), (2018) 672–677. https://doi.org/10.1049/iet-map.2017.0467

[19] N. Shoaib, S. Shoaib, R.Y. Khattak, I. Shoaib, X. Chen, A. Perwaiz, MIMO antennas for smart 5G devices. IEEE access, 6, (2018) 77014-77021. https://doi.org/10.1109/ACCESS.2018.2876763

[20] A.A.R.Saad, H.A. Mohamed, Printed millimeter-wave MIMO-based slot antenna arrays for 5G networks. AEU-International Journal of Electronics and Communications, 99, (2019) 59-69. https://doi.org/10.1016/j.aeue.2018.11.029

[21] H.Jiang, L.M. Si, W. Hu, X. Lv, A symmetrical dual-beam bowtie antenna with gain enhancement using metamaterial for 5G MIMO applications. IEEE Photonics Journal, 11(1),

(2019) 1-9. https://doi.org/10.1109/JPHOT.2019.2891003

[22] L. Liu, S.W. Cheung, Y.F. Weng, T.I. Yuk, M. Matin, (2012). Cable effects on measuring small planar UWB monopole antennas. In Ultra Wideband—Current Status and Future Trends, London. https://doi.org/10.5772/46080

[23] L. Liu, Y.F. Weng, S.W. Cheung, T.I. Yuk, L.J. Foged, (2011) Modeling of cable for measurements of small monopole antennas. In 2011 Loughborough Antennas & Propagation Conference, IEEE, UK. https://doi.org/10.1109/LAPC.2011.6114153

[24] S.H. Chae, S. Oh, S. Park, Analysis of mutual coupling, correlations, and TARC in WiBro MIMO array antenna. IEEE Antennas and Wireless Propagation Letters, 6, (2007) 122–125. https://doi.org/10.1109/LAWP.2007.893109

[25] M. Khalid, S. Iffat Naqvi, N. Hussain, M. Rahman, Fawad, S.S. Mirjavadi, M.J. Khan, Y. Amin, 4-Port MIMO antenna with defected ground structure for 5G millimeter wave applications. Electronics, 9(1), (2020) 71. https://doi.org/10.3390/electronics9010071

Authors Contribution Statement

Both the authors equally contributed and approved the final version of this work.

Funding

The authors declare that no funds, grants or any other support were received during the preparation of this manuscript.

Competing Interests

The authors declare that there are no conflicts of interest regarding the publication of this manuscript.

Data Availability

The data supporting the findings of this study can be obtained from the corresponding author upon reasonable request.

Has this article screened for similarity?

Yes